





Modest Effects of Osteoclast-Specific ER α Deletion after Skeletal Maturity

Madison L. Doolittle,¹ Brittany A. Eckhardt,¹ Stephanie J. Vos,¹ Sarah Grain,¹ Jennifer L. Rowsey,¹ Ming Ruan,¹ Dominik Saul,^{1,2}  Joshua N. Farr,¹  Megan M. Weivoda,³ Sundeep Khosla,¹  and David G. Monroe¹ 

¹Robert and Arlene Kogod Center on Aging and Division of Endocrinology, Mayo Clinic College of Medicine, Rochester, Minnesota, USA

²Department of Trauma and Reconstructive Surgery, Eberhard Karls University Tübingen, BG Trauma Center Tübingen, Tübingen, Germany

³Robert and Arlene Kogod Center on Aging and Division of Hematology, Mayo Clinic College of Medicine, Rochester, Minnesota, USA

ABSTRACT

Estrogen regulates bone mass in women and men, but the underlying cellular mechanisms of estrogen action on bone remain unclear. Although both estrogen receptor (ER) α and ER β are expressed in bone cells, ER α is the dominant receptor for skeletal estrogen action. Previous studies using either global or cell-specific ER α deletion provided important insights, but each of these approaches had limitations. Specifically, either high circulating sex steroid levels in global ER α knockout mice or the effects of deletion of ER α during growth and development in constitutive cell-specific knockout mice have made it difficult to clearly define the role of ER α in specific cell types in the adult skeleton. We recently generated and characterized mice with tamoxifen-inducible ER α deletion in osteocytes driven by the 8-kb *Dmp1* promoter (ER α Δ Ocy mice), revealing detrimental effects of osteocyte-specific ER α deletion on trabecular bone volume (–20.1%) and bone formation rate (–18.9%) in female, but not male, mice. Here, we developed and characterized analogous mice with inducible ER α deletion in osteoclasts using the *Cathepsin K* promoter (ER α Δ Ocl mice). In a study design identical to that with the previously described ER α Δ Ocy mice, adult female, but not male, ER α Δ Ocl mice showed a borderline (–10.2%, $p = 0.084$) reduction in trabecular bone volume, no change in osteoclast numbers, but a significant increase in serum CTx levels, consistent with increased osteoclast activity. These findings in ER α Δ Ocl mice differ from previous studies of constitutive osteoclast-specific ER α deletion, which led to clear deficits in trabecular bone and increased osteoclast numbers. Collectively, these data indicate that in adult mice, estrogen action in the osteocyte is likely more important than via the osteoclast and that ER α deletion in osteoclasts from conception onward has more dramatic skeletal effects than inducible osteoclastic ER α deletion in adult mice. © 2023 The Authors. *JBMR Plus* published by Wiley Periodicals LLC on behalf of American Society for Bone and Mineral Research.

KEY WORDS: ESTROGENS AND SELECTIVE ESTROGEN RECEPTOR MODULATOR; GENETIC ANIMAL MODELS; OSTEOCLASTS; OSTEOPOROSIS; SEX STEROIDS

Introduction

Although estrogen has been shown to be the major sex steroid regulating bone mass in women and men,⁽¹⁾ the cellular targets and underlying mechanisms of estrogen action on bone remain to be fully defined. As in other tissues, bone cells express both estrogen receptor (ER) α and ER β , but ER α appears to be the dominant receptor regulating bone metabolism.^(2,3) Different groups have assessed the skeletal consequences of deleting ER α both globally and specifically in osteoprogenitors,⁽⁴⁾ osteoblasts/osteocytes,^(5–7) osteoclasts,^(8,9) and immune cells.⁽¹⁰⁾ Although these models are informative, a potential problem with them is that the deletion of

ER α occurs from conception onward. Because postmenopausal osteoporosis is caused by a loss of estrogen signaling in adulthood, after the skeleton has fully matured, the relevance of these previous studies is difficult to translate to human physiology.

To address this problem, we previously developed and characterized mice with inducible ER α deletion in osteocytes using the 8-kb *Dmp1* promoter.⁽¹¹⁾ This model demonstrated important similarities and differences in skeletal phenotype compared to mice with constitutive osteocytic ER α deletion.^(5–7) Here, we develop and phenotype mice with inducible ER α deletion specifically in osteoclasts using the *Cathepsin K* (*Ctsk*) promoter. We then contrast the skeletal phenotypes of these mice to our previous osteocyte-specific

This is an open access article under the terms of the [Creative Commons Attribution](#) License, which permits use, distribution and reproduction in any medium, provided the original work is properly cited.

Received in original form February 27, 2023; revised form June 15, 2023; accepted June 28, 2023.

Address correspondence to: David G. Monroe, PhD, Mayo Clinic, Guggenheim 7, 200 First Street SW, Rochester, MN, 55905, USA.

E-mail: monroe.david@mayo.edu Sundeep Khosla, MD, Mayo Clinic, Guggenheim 7, 200 First Street SW, Rochester, MN, 55905, USA. E-mail: khosla.sundeep@mayo.edu

Additional supporting information may be found online in the Supporting Information section.

JBMR[®] Plus (WOA), Vol. 7, No. 10, October 2023, e10797.

DOI: 10.1002/jbm4.10797

© 2023 The Authors. *JBMR Plus* published by Wiley Periodicals LLC on behalf of American Society for Bone and Mineral Research.

inducible model,^(5–7) as well as to the previously described models of osteoclast-specific constitutive ER α deletion.^(8,9)

Materials and Methods

ER $\alpha^{fl/fl}$ and TdTomato mice

ER $\alpha^{fl/fl}$ mice were previously described and characterized.^(11,12) In these mice, exon 3 of the mouse ER α is flanked by lox P recombination sites. All mice used in this study, including these mice, were in the C57BL/6 background. The TdTomato mouse strain (B6;129S6-Gt(ROSA)26Sor^{tm9(CAG-tdTomato)Hze/JJAi9})⁽¹³⁾ was obtained from Jackson Laboratory under stock no. 007905.

Ctsk-CreERT2 construct design and transgenic mouse production

We developed an inducible osteoclast-specific Cre model using a validated *Ctsk* promoter described previously by the Davey group, which has been shown to have high specificity for osteoclasts.⁽¹⁴⁾ This promoter consists of nucleotides –3359 to +1660 of the *Ctsk* gene.⁽¹⁴⁾ The *Ctsk-CreERT2* construct was made by polymerase chain reaction (PCR) amplifying 5.1 kb of the *Ctsk* promoter in mouse genomic DNA using LongAmp *Taq* DNA Polymerase (New England Biolabs, Ipswich, MA, USA). This product was blunt-end cloned into the *Pme*I and *Hpa*I sites of the *attB*-containing pBT378 plasmid,⁽¹⁵⁾ with a 3' *Mlu*I site incorporated to facilitate the next cloning step. The CreERT2 gene was PCR amplified from *pCAG-CreERT2* (Addgene, Watertown, MA, USA) and cloned into this 3' *Mlu*I site to produce the final *Ctsk-CreERT2* construct. Transgenic mice were produced through the Stanford Transgenic, Knockout and Tumor Model Center by selectively inserting the *Ctsk-CreERT2* construct into the ROSA locus in C57BL/6 mice using integrase-mediated transgenesis.⁽¹⁵⁾ This technique assures a high efficiency of a single-copy transgene insertion into a predetermined and transcriptionally active chromosome locus.

Mouse husbandry and genetic crosses

Animal studies were conducted in accordance with National Institutes of Health (NIH) guidelines and with approval from the Institutional Animal Care and Use Committee (IACUC) at the Mayo Clinic, with all assessments performed in a blinded fashion. We used both male and female adult mice (aged 4 months, collected at 5 months) for our experimental procedures. To generate experimental mice, heterozygous *CtskCreERT2* males were bred with homozygous ER $\alpha^{fl/fl}$ females to generate *CtskCreERT2*+/-/ER $\alpha^{fl/fl}$ + heterozygotes. Sires from this cross were then bred to ER $\alpha^{fl/fl}$ + mice to generate *CtskCreERT2*+/-/ER $\alpha^{fl/fl}$ and *CtskCreERT2*+/- groups. All mice phenotyped were littermates.

Tamoxifen treatments

Tamoxifen (Sigma-Aldrich, St. Louis, MO, USA) was dissolved in 98% corn oil, 2% ethanol to 10 mg/mL and delivered subcutaneously at a dose of 50 mg/kg. In *TdTomato* experiments, 4-month-old *CtskCreERT2* \times *TdTomato* mice were injected with either corn oil or tamoxifen for five consecutive days (D1–5), then intermittently (D15 and D22) before sacrifice (D31). This dosing scheme was similarly used for the experimental phenotyping studies. Due to tamoxifen effects on bone metabolism,^(16,17) all mice were treated with tamoxifen.

Tissue collection

Mice were anesthetized (ketamine/xylazine) and blood was collected by cardiac puncture and stored at –80°C. The L4–L6 lumbar vertebrae were dissected, cleaned, and stored in ethanol for micro-computed tomography (μ CT). Right femurs were embedded in methyl methacrylate (MMA) for bone histomorphometry. Both tibiae and the thoracic vertebrae were isolated and cleaned, and marrow-free bone samples were obtained using centrifugation, as described previously.⁽¹⁸⁾ Samples were homogenized in QIAzol Lysis reagent (QIAGEN, Valencia, CA, USA) and stored at –80°C.

TdTomato histology and staining

Femur, lumbar spine, and soft tissues were fixed in 4% paraformaldehyde (PFA) at 4°C for 72 h under gentle agitation. Bones were decalcified in 10% EDTA for 2 weeks at 4°C under gentle shaking agitation, followed by incubation in 30% sucrose for 3 days at 4°C. Samples were embedded in Cryomatrix (Thermo Fisher Scientific, Wilmington, DE, USA) and flash frozen in liquid nitrogen and stored at –80°C. Cryosections 7 μ m thick were prepared for fluorescent imaging. Bone sections were stained for tartrate-resistant acid phosphatase (TRACP) activity to detect osteoclasts using a fluorescent phosphatase substrate (ELF97).⁽¹⁹⁾ ELF97 was dissolved 1:25 in TRACP staining solution (1 mM sodium nitrite, 100 mM acetate, and 7.4 mM tartrate), and sections were stained for 15 min at 37°C. Sections were mounted with ProLong Antifade (Thermo Fisher Scientific, Waltham, MA, USA) and all slides were imaged using the Zeiss Axio Observer Z1 microscope (Carl Zeiss Microscopy, LLC) and ZenPro software (Carl Zeiss Microscopy, LLC).

RNAscope analyses

In situ hybridization of ER α mRNA in osteoclasts was performed on FFPE bone sections ($n = 4$ per group) from the lumbar spine using the RNAscope 2.5 HD Reagent kit (Advanced Cell Diagnostics [ACD], Newark, CA, USA). Then 5- μ m-thick paraffin sections were deparaffinized, followed by Pepsin Reagent (Sigma) antigen retrieval for 30 min at 37°C. Target probes for ER α (*Esr1*) (Catalog No. 478201, ACD) and *Oscar* (Catalog No. 1179641-C1, ACD) were used with the RNAscope procedure followed according to the manufacturer's instructions. Sections were mounted (VectaMount, Vector Laboratories, Burlingame, CA, USA) and visualized using a $\times 40$ objective of the Nikon Eclipse T1 microscope. Approximately 200 osteoclasts were counted per section (in 30 separate fields of view) and scored for ER α positivity.

Quantitative PCR (qPCR) analysis

Total RNA was extracted using RNeasy Mini Columns with DNase solution (QIAGEN). Reverse transcriptase was performed with the High-Capacity cDNA Reverse Transcription Kit (Applied Biosystems by Life Technologies, Foster City, CA, USA). qRT-PCR was performed on the ABI Prism 7900HT Real Time System (Applied Biosystems, Carlsbad, CA, USA) using SYBR green (QIAGEN). The mouse primer sequences are provided in Table S1. Input RNA was normalized using housekeeping genes (*Actb*, *Gapdh*, *Hprt*, *Tuba1a*, *Tbp*) from which the most stable reference gene was determined by the geNorm algorithm.⁽²⁰⁾ The delta Ct for each gene was used to calculate the relative mRNA expression

changes for each sample. Genes with Ct values above 35 were considered not expressed, as was done previously.⁽²¹⁾

Skeletal phenotyping

μ CT imaging was performed on a Viva Scan 40 μ CT scanner (Scanco Medical AG, Basserdorf, Switzerland) with the following parameters: 55 kVp, 145 mA, high resolution, 21.5 diameter, 10.5- μ m voxel size, 300-ms integration time. Longitudinal analysis of bone microarchitecture was performed on the tibial diaphysis at baseline (4 months) and endpoint (5 months) before sacrifice. Animals were anesthetized using 2% to 4% isoflurane inhalation for induction and 1% isoflurane for maintenance and remained immobilized for the entirety of the scan. In each mouse, the distal epiphysis of the tibia was identified (specifically the tibia/fibula junction), and diaphysis scans were initiated 1 mm proximal to this anatomical landmark. Cortical parameters were assessed at the tibial midshaft diaphysis (50 slices). Ex vivo quantitative analysis of the lumbar spine (L5) was performed on dissected tissue after sacrifice. Three-dimensional analysis was used to calculate morphometric parameters at the lumbar vertebral body (200 slices) defining trabecular bone mass and microarchitecture.

Bone histomorphometry

All histological analyses were done in a blinded fashion. For dynamic histomorphometry, mice were injected subcutaneously

with Alizarin-3-methyliminodiacetic acid (0.1 mL/animal, 7.5 mg/mL) and calcein (0.1 mL/animal, 2.5 mg/mL) on days 9 and 2, respectively, before euthanasia. Bone sectioning and histomorphometry were performed as previously described.⁽³⁾

Serum protein measurements

Blood was drawn from cardiac bleeds from overnight fasted mice. Cardiac blood was allowed to clot, and serum was collected by centrifugation at 8500 rpm for 5 min at room temperature. Bone marker assays were conducted for PINP (amino-terminal propeptide of type I collagen) using the Rat/Mouse PINP enzyme immunoassay (EIA) kit (Immuno Diagnostic Systems [IDS], Scottsdale, AZ, USA) and CTx (cross-linked C-telopeptide of type I collagen) using the RatLaps Rat/Mouse CTx EIA kit (IDS). Serum E₂ was measured by liquid chromatography–mass spectrometry (LC–MS)/MS (API 5000, Applied Biosystems–MDS Sciex; interassay CV 8%).

Statistical analyses

Statistically significant differences were determined in Graphpad Prism version 9.3.1 (GraphPad Software, Inc., La Jolla, CA, USA) and R (version 4.0.3). All data were tested for normality using the Shapiro–Wilk test, and for parametric data we performed an unpaired *t*-test. Experimental group numbers are indicated in each figure. Mouse group sizes were based on previously conducted and published experiments.^(3,11)

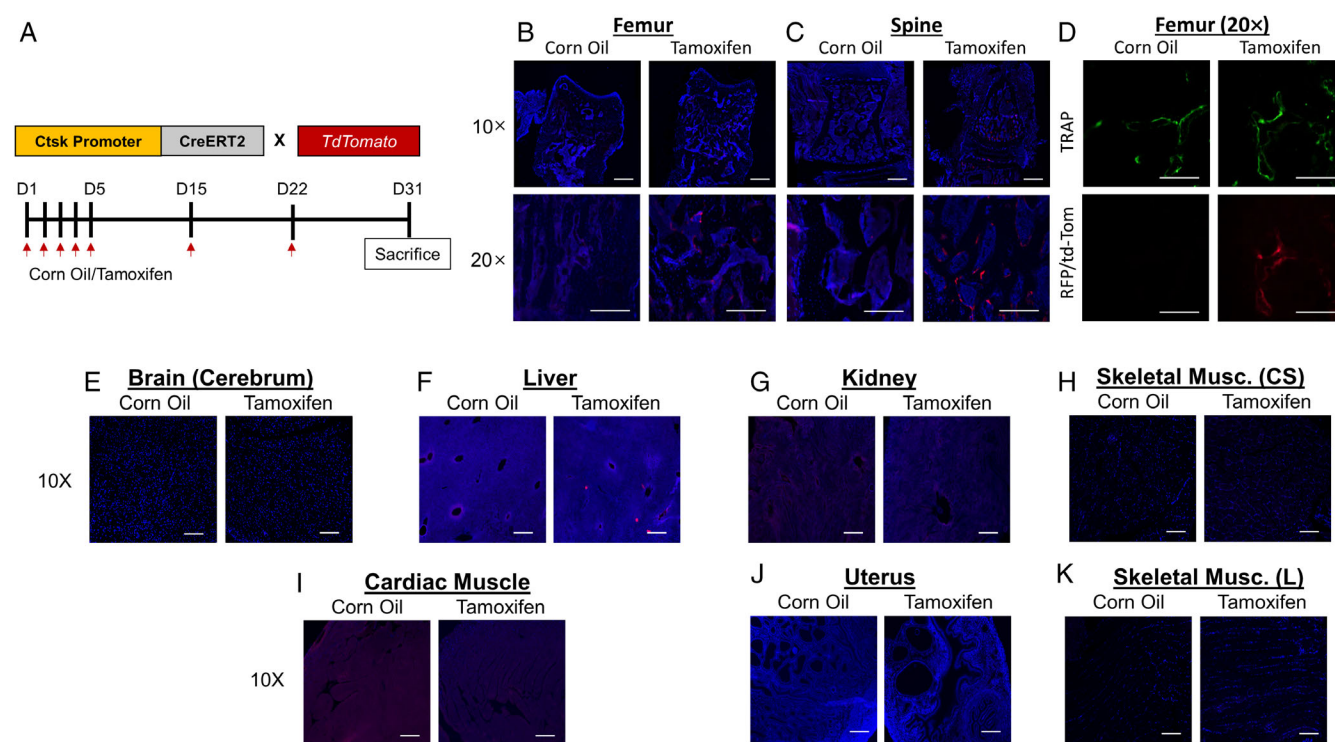


Fig. 1. The *Ctsk-CreERT2* mouse model targets osteoclasts. (A) Experimental outline for model validation in *Ctsk-CreERT2* × *TdTomato* mice. (B) Representative images of induced TdTomato expression in osteoclasts in femur and (C) spine of corn oil- versus tamoxifen-treated *Ctsk-CreERT2* × *TdTomato* mice at low (×10) and high (×20) magnification. (D) Fluorescent TRACP staining of femur sections indicating overlap with TdTomato+ cells. (E–L) Representative images of induced TdTomato expression in various soft tissues of corn oil- versus tamoxifen-treated *Ctsk-CreERT2* × *TdTomato* mice. CS = cross section; L = longitudinal. Scale bars = 100 μ m.

Results

Construction of osteoclast-specific Ctsk-CreERT2 model

Generation of the *Ctsk-CreERT2* mice is described in detail in the Methods section. The *Ctsk-CreERT2* mice were crossed with Ai9 *TdTomato* mice and treated with tamoxifen (Fig. 1A) to evaluate specificity for osteoclasts. In the tamoxifen-treated mice, but not the corn oil-treated control mice, we observed selective recombination on the surfaces of trabecular bone in the femur and spine (Fig. 1B,C). For specificity for osteoclasts, we next performed fluorescent TRACP staining, demonstrating colocalization of TRACP and *TdTomato* in the tamoxifen- but not in the corn oil-treated mice (Fig. 1D). To evaluate the possible expression of Cre in the *Ctsk-CreERT2* mice in cells other than osteoclasts, we evaluated a number of other tissues, finding no evidence of Cre expression in brain, kidney, uterus, and skeletal as well as cardiac muscle, with minimal recombination in the liver (Fig. 1E–K). We also examined femoral bone sections for periosteal Ctsk expression, since these cells arise from the Groove of Ranvier and are Ctsk positive. As seen in Fig. S1, TdTomato signal is only observed on endosteal bone surfaces.

Validation of Ctsk-CreERT2-mediated ER α deletion in adult mice

We next crossed the *Ctsk-CreERT2* mice with mice homozygous for a floxed allele of the gene encoding estrogen receptor α (*ER α ^{fl/fl}*)

^{fl/fl}(12) to create mice with inducible deletion of ER α in osteoclasts following tamoxifen treatment (“*ER α Δ Ocl*” mice; see Methods for breeding strategy) (Fig. 2A). Given the known effects of tamoxifen on bone,^(16,17) we used control mice that were *CreERT2* only, which were treated with identical doses of tamoxifen. Because global deletion of ER α in mice leads to elevated circulating estrogen levels secondary to hypothalamic–pituitary feedback,⁽²²⁾ we also measured serum estradiol levels, which were no different in the control versus the *ER α Δ Ocl* mice (Fig. 2B).

Given that osteoclasts constitute only a minority of cells in the bone microenvironment and are relatively difficult to isolate using flow sorting, we used in situ hybridization (RNAScope) to measure *ER α* mRNA along with the osteoclast-specific marker *Oscar*⁽²³⁾ to demonstrate the efficacy of osteoclast-specific *ER α* deletion in the *ER α Δ Ocl* mice. Using this approach, we were able to clearly demonstrate a significant reduction in the *ER α* mRNA in *Oscar*-expressing osteoclasts (Fig. 2C,D). Specifically, we found that the percentage of *ER α* + osteoclasts decreased from $52.3 \pm 12.7\%$ in the control mice to $32.5 \pm 3.0\%$ in the *ER α Δ Ocl* mice ($p = 0.023$). Although the reduction was modest, we note that its magnitude in *ER α* + osteoclasts in the inducible *ER α Δ Ocl* mice was almost identical to the reduction of *ER α* + osteocytes that we recently observed in a parallel model for osteocyte-specific *ER α* deletion using the 8-kb *Dmp1* promoter (*ER α Δ Ocy*),⁽¹¹⁾ where we nonetheless observed substantial deficits in trabecular bone in female mice following inducible osteocytic *ER α* deletion.

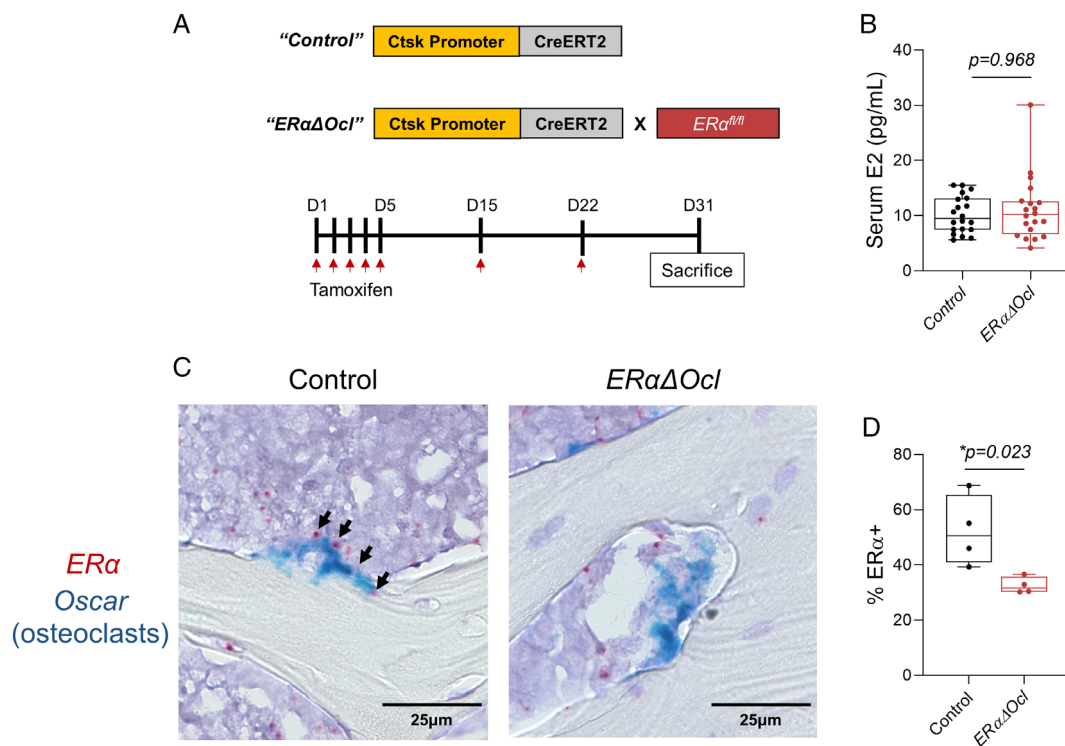


Fig. 2. Validation of osteoclast-specific ER α deletion in adult *ER α Δ Ocl* mice. (A) Experimental outline for inducible deletion of ER α in *Ctsk* + osteoclasts. (B) Measurement of serum estradiol (E2) from cardiac blood ($n = 15$ – 16 per group). (C) RNAScope images of *Esr1* (red: encoding ER α) and osteoclast-specific *Oscar* (blue) mRNA probes performed on spine bone sections from tamoxifen-treated *ER α Δ Ocl* mice. Magnification $\times 40$, scale bars = $25 \mu\text{m}$. Black arrows point to ER α positivity on osteoclasts. (D) Quantification of percentage of *Oscar* + osteoclasts positive for ER α observed from RNAScope ($n = 4$ per group; two male, two female). Statistical significance was determined by unpaired *t*-test.

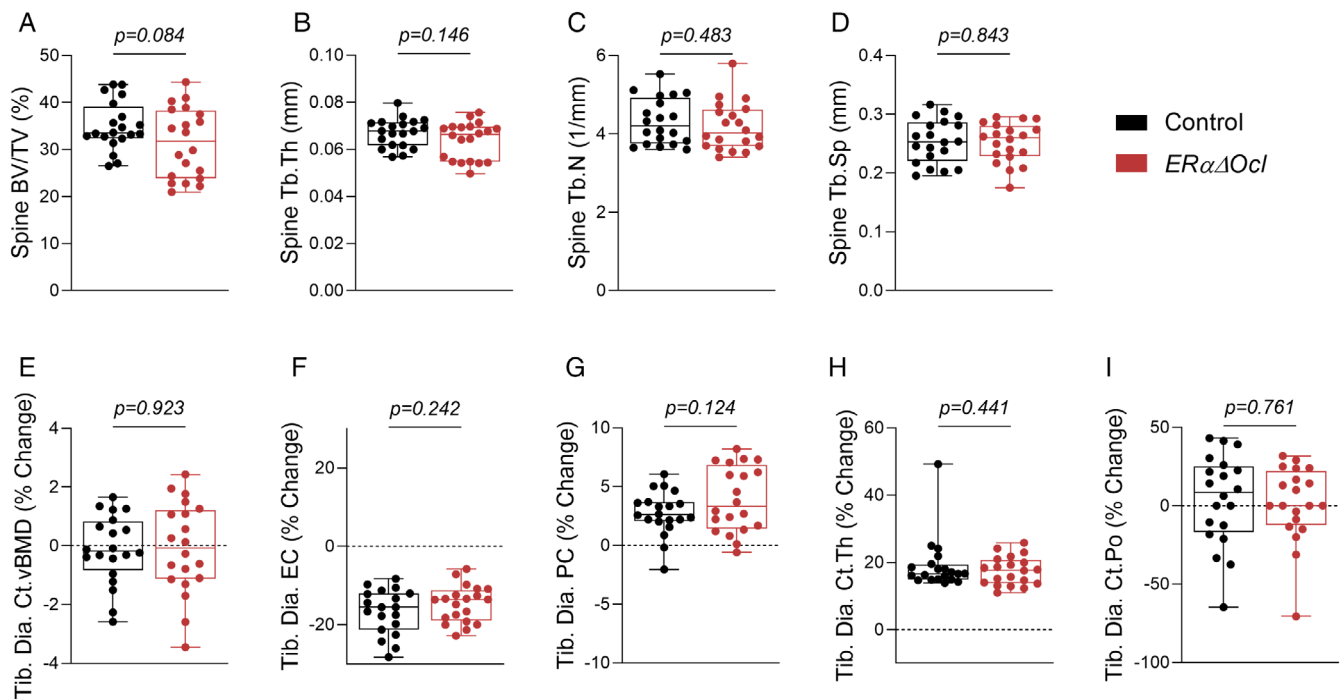


Fig. 3. Osteoclast-specific deletion of ER α in adult female mice does not alter bone mass. μ CT analyses of lumbar spine demonstrating (A) bone volume fraction (BV/TV), (B) trabecular thickness (Tb.Th), (C) trabecular number (Tb.N), and (D) trabecular spacing (Tb.Sp). (E–I) Longitudinal μ CT analyses of cortical bone at tibial diaphysis (Tib. Dia.) showing percentage (%) change between baseline and endpoint. (E) Cortical volumetric BMD (vBMD), (F) endocortical circumference (EC), (G) periosteal circumference (PC), (H) cortical thickness (Ct.Th), and (I) cortical porosity (Ct.Po). $n = 19$ –20 mice per group. Statistical significance was determined by unpaired t -test.

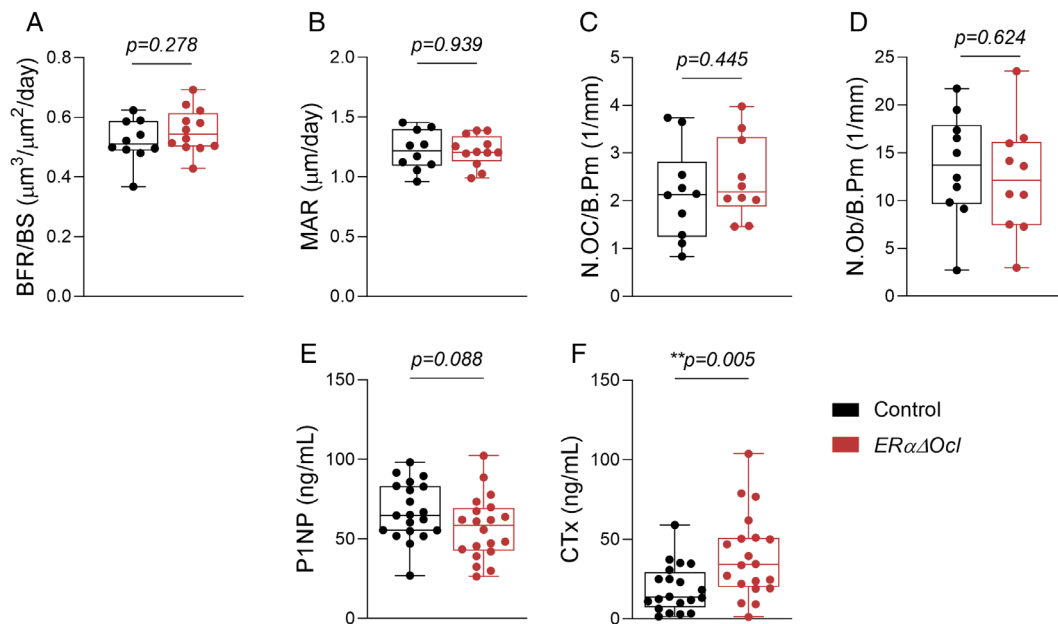


Fig. 4. ER α deletion in osteoclasts does not affect bone formation or resorption but may increase osteoclast activity. (A) Measurement of bone formation rate per bone surface (BFR/BS) and (B) mineral apposition rates (MARs) in lumbar spines of female $ER\alpha\Delta Ocl$ and control mice using double-label dynamic histomorphometry. (C) Counted number of osteoclasts (N.OC/B.Pm) and (D) osteoblasts (N.OB/B.Pm) normalized to bone perimeter using static histomorphometry. (E, F) Dynamic histomorphometry measurements in female $ER\alpha\Delta Ocl$ and control mice. (F–H) Osteoclast and osteoblast numbers in $ER\alpha\Delta Ocl$ and control mice. Statistical significance determined by unpaired t -test. (A–D) $n = 10$ –12 per group, (E, F) $n = 19$ –20 per group.

Skeletal phenotyping of $ER\alpha\Delta Ocl$ mice

As noted in the preceding discussion, due to the known effects of tamoxifen on bone,^(16,17) we compared the skeletal phenotypes of the $ER\alpha\Delta Ocl$ mice to control *Ctsk-CreERT2* mice treated identically with tamoxifen. Four-month-old $ER\alpha\Delta Ocl$ and control mice were treated with the tamoxifen regimen and assessed for skeletal effects at 5 months of age (Fig. 1A). In female $ER\alpha\Delta Ocl$ mice, we observed a nonsignificant trend (-10.2% , $p = 0.084$) for a reduction in spine bone volume fraction (BV/TV, Fig. 3A), but no other changes in spine trabecular bone (Fig. 3B–D). Next, we assessed changes in cortical bone parameters through longitudinal μCT of the tibial diaphysis. We found no changes in cortical volumetric BMD (vBMD) or alterations in rates of endocortical or periosteal apposition in the $ER\alpha\Delta Ocl$ mice (Fig. 3E–G), while also observing no change in cortical thickness or porosity (Fig. 3H,I). Note that tibial endocortical diameter was decreased and periosteal diameter was increased in both the control and $ER\alpha\Delta Ocl$ mice, likely reflecting an effect of tamoxifen through $ER\alpha$ in cells other than osteoclasts.

In male mice, we also observed no change in spine trabecular BV/TV or other parameters in $ER\alpha\Delta Ocl$ mice (Fig. S2A,D), other than a minor increase in spine trabecular thickness (Tb.Th) and

a concordant reduction in trabecular spacing (Tb.Sp) (Fig. S2B,D). Interestingly, in male $ER\alpha\Delta Ocl$ mice relative to control mice, we observed endocortical surface expansion in the tibia, in addition to reduced overall cortical thickness as measured by longitudinal μCT (Fig. S1E,F). This was accompanied by no change in periosteal surface diameter, cortical vBMD, or cortical porosity (Fig. S1G–I).

Alterations in cellular function in $ER\alpha\Delta Ocl$ mice

To investigate any alterations in bone formation or resorption that might explain the skeletal phenotype, we performed static and dynamic bone histomorphometry in $ER\alpha\Delta Ocl$ mice. We focused on female mice where previous studies on noninducible osteoclast-specific $ER\alpha$ deletion showed clear skeletal effects.^(8,9) In the $ER\alpha\Delta Ocl$ mice, there were no significant changes in bone formation (Fig. 4A) or mineral apposition (Fig. 4B) rates. Additionally, both osteoclast and osteoblast numbers were unchanged relative to control mice (Fig. 4C,D). Interestingly, although serum P1NP levels (bone formation) were unchanged (Fig. 4F), there was a significant increase in serum CTx levels (bone resorption) in the $ER\alpha\Delta Ocl$ mice. This finding, in the context of a lack of changes in osteoclast numbers (Fig. 4C) and a trend toward

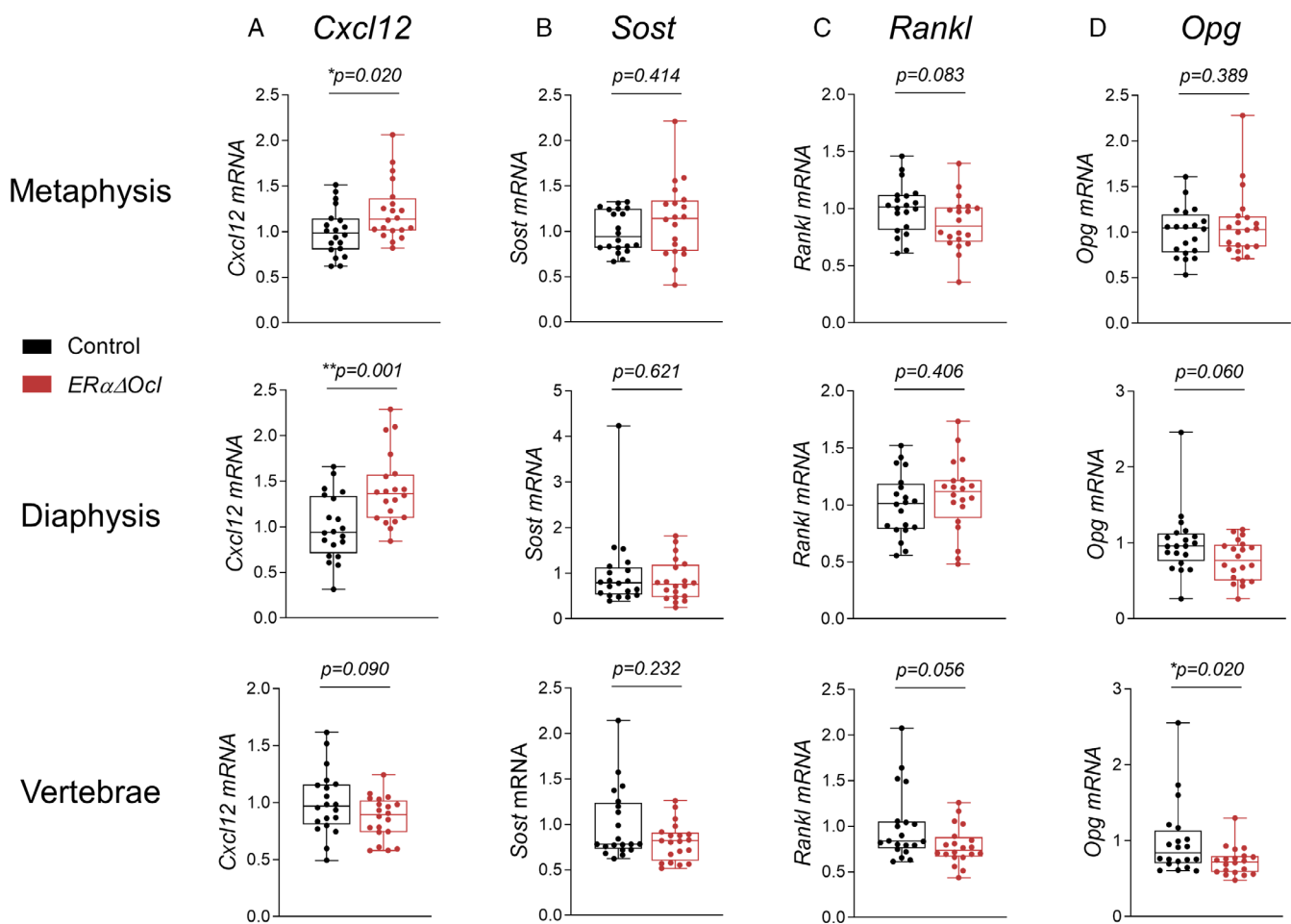


Fig. 5. $ER\alpha\Delta Ocl$ mice display increased *Cxcl12* expression yet exhibit no change in osteoblast-derived bone turnover genes. mRNA expression of (A) *Cxcl12*, (B) *Sost*, (C) *Rankl*, and (D) *Opg* in $ER\alpha\Delta Ocl$ mice (fold-change relative to control group) at femur diaphysis, metaphysis, and thoracic spine. $n = 20$ mice per group. Statistical significance determined by unpaired t-test.

Table 1. Phenotypic comparison of inducible versus constitutive ER α deletion in osteocytes and osteoclasts

	Inducible ER α deletion (5 months)		Constitutive ER α deletion	
	ER α Δ Ocl	ER α Δ Ocy ⁽¹¹⁾	Ctsk-Cre ⁽⁸⁾	LysM-Cre ⁽⁹⁾
BV/TV (spine)	=	↓	↓ (12 weeks)	↓ (22 weeks)
N.Oc/B.Pm	=	↑	↑	↑
CTx (serum)	↑	=	ND	ND

Note: BV/TV = bone volume fraction; N.Oc/B.Pm = osteoclast number per bone perimeter; “=” = no change; ↑ = parameter increases; ↓ = parameter decreases; ND = parameter not determined.

decreased spine BV/TV (Fig. 3A), indicates that inducible ER α deletion results in an increase in osteoclast activity, but not in osteoclast numbers.

Previous studies using constitutive ER α deletion in osteoblast lineage cells (using the Prx1-Cre⁽²⁴⁾) as well as inducible ER α deletion in osteocytes in our parallel model (ER α Δ Ocy⁽¹¹⁾) demonstrated significant increases in the pro-osteoclastogenic cytokine, Cxcl12 (SDF-1),⁽²⁵⁾ in the bones of ER α knockout mice. Of interest, we found increased Cxcl12 mRNA levels in the femur metaphysis and diaphysis in ER α Δ Ocl mice (Fig. 5A). By contrast, Sost, which was markedly increased in the bones of the ER α Δ Ocy mice,⁽¹¹⁾ was unchanged in ER α Δ Ocl mice (Fig. 5B). Notably, bone Opg mRNA levels were significantly reduced in the vertebrae of the ER α Δ Ocl mice, with a similar trend for Rankl (Fig. 5C,D).

Discussion

In this study, we developed and validated a new tamoxifen-inducible Cre model targeting osteoclasts, analogous to our previous inducible model targeting osteocytes.⁽¹¹⁾ In adult mice, the Ctsk-CreERT2 appears to be highly specific for osteoclasts; importantly, Cre activation by tamoxifen at 4 months of age avoided issues related to Ctsk expression in mesenchymal cells in the groove of Ranvier⁽²⁶⁾ or in periosteal cells⁽²⁷⁾ that may occur during embryonic or early postnatal development.

As previously recognized by Kedlaya and colleagues for the 10-kb Dmp1-CreERT2 model⁽²⁸⁾ and by us for the 8-kb Dmp1-CreERT2 mice,⁽¹¹⁾ it is challenging to demonstrate deletion of target genes in inducible Cre models. Even though we used the Ai9 TdTomato reporter mice to demonstrate specificity for osteoclasts, reliance solely on reporter mice is problematic since gene deletions with a given Cre can vary substantially from one floxed gene to another, likely due to local chromatin structure around floxed alleles.⁽²⁹⁾ In addition, given the relatively low abundance of osteoclasts within bone, assessing the extent of gene deletion using DNA rearrangement or mRNA levels in whole bone lacks sufficient sensitivity due to the overwhelming number of contaminating cells not expressing Cre. As such, similar to our previous study with the ER α Δ Ocy model,⁽¹¹⁾ we used in situ hybridization (RNAScope) for the ER α transcript combined with an osteoclast-specific transcript (Oscar)⁽²³⁾ and demonstrated a modest (from 52.3% to 32.5%) but significant reduction in osteoclasts positive for ER α . Of note, this reduction in ER α + osteoclasts in the ER α Δ Ocl mice was remarkably similar to the reduction in ER α + osteocytes we previously demonstrated in our inducible osteocytic ER α deletion model (from 51.1% to 38.8%).⁽¹¹⁾

Despite a very similar extent of ER α deletion, the skeletal phenotype of the ER α Δ Ocl mice differed substantially from that of the identically treated ER α Δ Ocy mice.⁽¹¹⁾ We previously found

that female ER α Δ Ocy mice had significant reductions in spine BV/TV (−20.1%) accompanied by decreased trabecular bone formation rates (−18.9%). The female ER α Δ Ocy mice also had periosteal and endocortical expansion, but preserved cortical thickness, consistent with the known effects of estrogen to inhibit periosteal apposition and promote endocortical formation.⁽³⁰⁾ In addition, osteoclast numbers were increased in trabecular bone in the ER α Δ Ocy mice. By contrast, female ER α Δ Ocl mice had a minimal skeletal phenotype, with only a borderline reduction in spine BV/TV and no change in osteoclast numbers, although they did exhibit an increase in serum CTx levels, consistent with an increase in osteoclast activity. In males, both the ER α Δ Ocy and ER α Δ Ocl mice had fairly unremarkable skeletal phenotypes.

The phenotype of the inducible ER α Δ Ocl mice was also different from that of two previous constitutive osteoclast ER α deletion models using either Ctsk-Cre⁽⁸⁾ or LysM-Cre.⁽⁹⁾ As summarized in Table 1, constitutive Ctsk-Cre-mediated ER α deletion in female, but not male, mice led to trabecular osteopenia and increased osteoclast numbers by 12 weeks of age, with no alterations in cortical bone.⁽⁸⁾ The phenotype of the mice with LysM-Cre-mediated ER α deletion was slightly different, in that neither trabecular osteopenia nor increases in osteoclast numbers were evident at 12 weeks, but they were present by 22 weeks of age.⁽⁹⁾

Collectively, comparison of the skeletal phenotype of current inducible ER α Δ Ocl mice to that of the identically treated inducible ER α Δ Ocy mice, as well as the two constitutive osteoclast ER α models, is informative in several respects (Table 1). First, in adult mice with inducible ER α deletion, osteocytic ER α deletion clearly has more profound skeletal consequences than osteoclastic ER α deletion. Second, constitutive ER α deletion in osteoclasts from conception onward also has more profound skeletal consequences than inducible osteoclastic ER α deletion in adult mice studied over 1 month. There are several potential explanations for the discrepancies between the inducible and constitutive osteoclastic ER α deletion models. First, the effects of inducible osteoclastic ER α deletion may take longer to manifest than the 1-month time frame of the current study. Consistent with this, at least in the LysM-Cre ER α deletion model, there was no skeletal phenotype at 12 weeks of age, and the phenotype was only evident by 22 weeks of age.⁽⁹⁾ A second explanation may come from recent work showing that, in contrast to adult osteoclasts that are derived from hematopoietic stem cells, neonatal and early-life osteoclasts appear to have a different origin and are derived from erythromyeloid progenitor (EMP) cells.⁽³¹⁾ Thus, noninducible osteoclastic ER α deletion may target an entirely different osteoclast population, possibly influencing skeletal development, as compared to inducible osteoclastic ER α deletion in adult mice, which simulates postmenopausal loss of estrogen signaling. Finally, it is also plausible and perhaps

likely that the increased bone resorption in states of estrogen deficiency in adult mice is mainly caused by lack of ER α -mediated suppression of pro-resorptive factors (e.g., receptor activator of NF- κ B ligand) in mesenchymal skeletal cells rather than through direct actions on osteoclasts. Although we offer these explanations for the lack of a significant skeletal phenotype in the adult inducible *ER α Δ Ocl* mice, more studies are clearly needed to address these possibilities.

Our data also demonstrate that the inducible *Ctsk-CreERT2* mouse model only targets osteoclastic cells on endosteal bone surfaces and not periosteal bone surfaces. This is in contrast to the constitutive *Ctsk-Cre* mouse model, which clearly shows periosteal expression of Cre.⁽⁸⁾ These observations are consistent with the fact that the *Ctsk-CreERT2* inducible model is not active during development, whereas the constitutive *Ctsk-Cre* is active from conception onward, so this is a distinct advantage of the inducible model.

A compelling interpretation in examining the bone phenotypes of the two ER α inducible models can be drawn when considering the role of ER α in adult osteoclasts versus osteocytes, in terms of their role on osteoclasts themselves. As seen in the Results and briefly summarized in Table 1, in the inducible *ER α Δ Ocl* mice there is no effect on osteoclast number (N.Oc/B.Pm), but an increase in serum CTx is observed, whereas in the *ER α Δ Ocy* mice, the opposite is found. This suggests that the cellular pools of ER α in adult osteoclasts and osteocytes may function in different capacities, with the osteoclastic pool influencing osteoclast activity and the osteocytic pool influencing osteoclast number.

One of the limitations of this study is that the bone phenotype of the inducible *ER α Δ Ocl* mice was only measured at one time point (5 months of age), as it is possible that a more definitive phenotype would be observed in older mice. However, this time point was chosen to assess the potential phenotype in young adult mice and to mirror the experimental conditions of the *ER α Δ Ocy* mice,⁽¹¹⁾ in an effort to directly compare the skeletal consequences of inducible ER α deletion in osteoclasts and osteocytes, respectively. Future experiments examining the effects of these deletions in older mice may uncover important data not observed in this study.

In summary, we describe the development and validation of a new, tamoxifen-inducible *Ctsk-CreERT2* model that may circumvent a number of potential confounders of constitutive osteoclast-specific Cre models. When comparing these mice to analogous models with inducible osteocytic ER α deletion, as well as mice with constitutive osteoclastic ER α deletion, our data indicate that osteocytic ER α plays a more important role in regulating adult bone metabolism than osteoclastic ER α , at least in female mice. Our study also points to potential differences between deleting ER α (or potentially other genes) in osteoclasts from conception onward versus inducibly in adult mice.

Acknowledgments

This work was supported by NIH Grants P01 AG004875, AG062413 (to Sundeep Khosla/David G. Monroe), R01 AR068275 (to David G. Monroe), R01 AG063707 (to David G. Monroe), and R01 DK128552.

Author Contributions

Madison L. Doolittle: Conceptualization; data curation; formal analysis; investigation; methodology; writing – original draft;

writing – review and editing. **Brittany Eckhardt:** Investigation; methodology; writing – review and editing. **Stephanie Vos:** Investigation; methodology; writing – review and editing. **Sarah Grain:** Investigation; methodology; writing – review and editing. **Jennifer L. Rowsey:** Investigation; methodology; writing – review and editing. **Ming Ruan:** Investigation; methodology; writing – review and editing. **Dominik Saul:** Formal analysis; investigation; methodology; writing – review and editing. **Joshua N. Farr:** Investigation; methodology; writing – review and editing. **Megan Weivoda:** Investigation; methodology; writing – review and editing. **Sundeep Khosla:** Conceptualization; funding acquisition; project administration; supervision; writing – original draft; writing – review and editing. **David G. Monroe:** Conceptualization; data curation; formal analysis; funding acquisition; investigation; methodology; project administration; supervision; writing – original draft; writing – review and editing.

Disclosures

The authors have no relevant financial disclosures and no conflicts of interest.

Peer Review

The peer review history for this article is available at <https://www.webofscience.com/api/gateway/wos/peer-review/10.1002/jbm4.10797>.

Data Availability Statement

The data that support the findings of this study are available from the corresponding author upon request.

References

1. Khosla S, Melton LJ 3rd, Riggs BL. The unitary model for estrogen deficiency and the pathogenesis of osteoporosis: is a revision needed? *J Bone Miner Res*. 2011;26(3):441–451.
2. Khosla S, Monroe DG. Regulation of bone metabolism by sex steroids. *Cold Spring Harb Perspect Med*. 2018;8(1):a031211.
3. Nicks KM, Fujita K, Fraser D, et al. Deletion of estrogen receptor Beta in Osteoprogenitor cells increases trabecular but not cortical bone mass in female mice. *J Bone Miner Res*. 2016;31(3):606–614.
4. Almeida M, Iyer S, Martin-Millan M, et al. Estrogen receptor-alpha signaling in osteoblast progenitors stimulates cortical bone accrual. *J Clin Invest*. 2013;123(1):394–404.
5. Kondoh S, Inoue K, Igarashi K, et al. Estrogen receptor alpha in osteocytes regulates trabecular bone formation in female mice. *Bone*. 2014;60:68–77.
6. Melville KM, Kelly NH, Khan SA, et al. Female mice lacking estrogen receptor-alpha in osteoblasts have compromised bone mass and strength. *J Bone Miner Res*. 2014;29(2):370–379.
7. Windahl SH, Borjesson AE, Farman HH, et al. Estrogen receptor-alpha in osteocytes is important for trabecular bone formation in male mice. *Proc Natl Acad Sci USA*. 2013;110(6):2294–2299.
8. Nakamura T, Imai Y, Matsumoto T, et al. Estrogen prevents bone loss via estrogen receptor alpha and induction of Fas ligand in osteoclasts. *Cell*. 2007;130(5):811–823.
9. Martin-Millan M, Almeida M, Ambrogini E, et al. The estrogen receptor-alpha in osteoclasts mediates the protective effects of estrogens on cancellous but not cortical bone. *Mol Endocrinol*. 2010;24(2):323–334.

10. Fujiwara Y, Piemontese M, Liu Y, Thostenson JD, Xiong J, O'Brien CA. RANKL (receptor activator of NFkappaB ligand) produced by osteocytes is required for the increase in B cells and bone loss caused by estrogen deficiency in mice. *J Biol Chem*. 2016;291(48):24838–24850.
11. Doolittle ML, Saul D, Kaur J, et al. Skeletal effects of inducible ER α deletion in osteocytes in adult mice. *J Bone Miner Res*. 2022;37(9):1750–1760.
12. Feng Y, Manka D, Wagner KU, Khan SA. Estrogen receptor-alpha expression in the mammary epithelium is required for ductal and alveolar morphogenesis in mice. *Proc Natl Acad Sci USA*. 2007;104(37):14718–14723.
13. Madisen L, Zwingman TA, Sunken SM, et al. A robust and high-throughput Cre reporting and characterization system for the whole mouse brain. *Nat Neurosci*. 2010;13(1):133–140.
14. Chiu WS, McManus JF, Notini AJ, Cassady AI, Zajac JD, Davey RA. Transgenic mice that express Cre recombinase in osteoclasts. *Genesis*. 2004;39(3):178–185.
15. Tasic B, Hippenmeyer S, Wang C, et al. Site-specific integrase-mediated transgenesis in mice via pronuclear injection. *Proc Natl Acad Sci USA*. 2011;108(19):7902–7907.
16. Zhang Z, Park JW, Ahn IS, et al. Estrogen receptor alpha in the brain mediates tamoxifen-induced changes in physiology in mice. *Elife*. 2021;10:e63333.
17. Xie Z, McGrath C, Sankaran J, et al. Low-dose tamoxifen induces significant bone formation in mice. *JBMR Plus*. 2021;5(3):e10450.
18. Kelly NH, Schimenti JC, Patrick Ross F, van der Meulen MC. A method for isolating high quality RNA from mouse cortical and cancellous bone. *Bone*. 2014;68:1–5.
19. Filgueira L. Fluorescence-based staining for tartrate-resistant acid phosphatase (TRAP) in osteoclasts combined with other fluorescent dyes and protocols. *J Histochem Cytochem*. 2004;52(3):411–414.
20. Vandesompele J, De Preter K, Pattyn F, et al. Accurate normalization of real-time quantitative RT-PCR data by geometric averaging of multiple internal control genes. *Genome Biol*. 2002;3(7):003411.
21. Farr JN, Fraser DG, Wang H, et al. Identification of senescent cells in the bone microenvironment. *J Bone Miner Res*. 2016;31(11):1920–1929.
22. Sims NA, Dupont S, Krust A, et al. Deletion of estrogen receptors reveals a regulatory role for estrogen receptors-beta in bone remodeling in females but not in males. *Bone*. 2002;30(1):18–25.
23. Matsuo K, Irie N. Osteoclast-osteoblast communication. *Arch Biochem Biophys*. 2008;473(2):201–209.
24. Ucer S, Iyer S, Kim HN, et al. The effects of aging and sex steroid deficiency on the murine skeleton are independent and mechanistically distinct. *J Bone Miner Res*. 2017;32(3):560–574.
25. Wright LM, Maloney W, Yu X, Kindle L, Collin-Osdoby P, Osdoby P. Stromal cell-derived factor-1 binding to its chemokine receptor CXCR4 on precursor cells promotes the chemotactic recruitment, development and survival of human osteoclasts. *Bone*. 2005;36(5):840–853.
26. Yang W, Wang J, Moore DC, et al. Ptpn11 deletion in a novel progenitor causes metachondromatosis by inducing hedgehog signalling. *Nature*. 2013;499(7459):491–495.
27. Ruiz P, Martin-Millan M, Gonzalez-Martin MC, Almeida M, González-Macias J, Ros MA. CathepsinKCre mediated deletion of β catenin results in dramatic loss of bone mass by targeting both osteoclasts and osteoblastic cells. *Sci Rep*. 2016;6:36201.
28. Kedlaya R, Kang KS, Hong JM, et al. Adult-onset deletion of beta-catenin in (10kb)Dmp1-expressing cells prevents intermittent PTH-induced bone gain. *Endocrinology*. 2016;157(8):3047–3057.
29. Vooijs M, Jonkers J, Berns A. A highly efficient ligand-regulated Cre recombinase mouse line shows that LoxP recombination is position dependent. *EMBO Rep*. 2001;2(4):292–297.
30. Turner RT, Wakley GK, Hannon KS. Differential effects of androgens on cortical bone histomorphometry in gonadectomized male and female rats. *J Orthop Res*. 1990;8(4):612–617.
31. Yahara Y, Barrientos T, Tang YJ, et al. Erythromyeloid progenitors give rise to a population of osteoclasts that contribute to bone homeostasis and repair. *Nat Cell Biol*. 2020;22(1):49–59.